ACS OMEGA

http://pubs.acs.org/journal/acsodf

Article

Deep Learning Promotes the Screening of Natural Products with Potential Microtubule Inhibition Activity

Xiao-Nan Jia,[⊥] Wei-Jia Wang,[⊥] Bo Yin,[⊥] Lin-Jing Zhou, Yong-Qi Zhen, Lan Zhang, Xian-Li Zhou, Hai-Ning Song,* Yong Tang,* and Feng Gao*

Cite This: *ACS Omega* 2022, 7, 28334−28341

Read Online

ACCESS | Metrics & More | Article Recommendations | Supporting Information

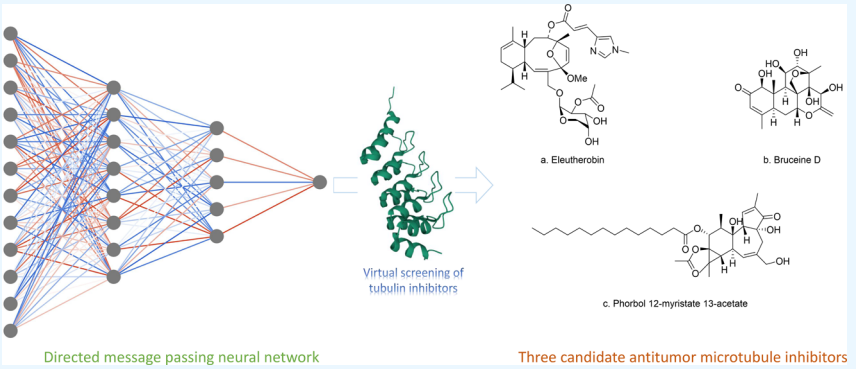

ABSTRACT: Natural microtubule inhibitors, such as paclitaxel and ixabepilone, are key sources of novel medications, which have a considerable influence on anti-tumor chemotherapy. Natural product chemists have been encouraged to create novel methodologies for screening the new generation of microtubule inhibitors from the enormous natural product library. There have been major advancements in the use of artificial intelligence in medication discovery recently. Deep learning algorithms, in particular, have shown promise in terms of swiftly screening effective leads from huge compound libraries and producing novel compounds with desirable features. We used a deep neural network to search for potent β-microtubule inhibitors in natural goods. Eleutherobin, bruceine D (BD), and phorbol 12-myristate 13-acetate (PMA) are three highly effective natural compounds that have been found as β-microtubule inhibitors. In conclusion, this paper describes the use of deep learning to screen for effective β-microtubule inhibitors. This research also demonstrates the promising possibility of employing deep learning to develop drugs from natural products for a wider range of disorders.

1. INTRODUCTION

Natural products are always an important source of new drugs.[1] Many famous drugs have been developed from plants, microbial metabolites, and marine organisms. Natural products play a vital role in the discovery and development of drugs, which are particularly evident in anti-tumor drugs. At present, more than 60% of anti-tumor drugs are closely related to natural products.[2] However, precise and efficient characterization of their biological effects remains challenging as the number of newly discovered natural products exponentially increased.[3] Therefore, without incurring the unsustainable costs of simply scaling typical discovery processes in parallel, artificial intelligence-assisted natural drug design has also emerged.[4−6]

Recently, there has been a growing enthusiasm for using deep learning to advance drug discovery.[7−9] Deep learning has been successfully applied in compound property prediction,[10,11] de novo design,[12−14] lead discovery,[15] repurposing,[16−18] and synthetic design.[19] Deep learning models demonstrate significant improvements in rapidly screening potent leads from massive compounds in available compound libraries. More recently, deep learning models achieved encouraging results in identifying antibacterial compounds,[18] candidates against osteoclastogenesis,[20] repurposing candidates for COVID-19.[21]

As a major target for chemotherapy of solid tumors, β-tubulin is essential for the growth and metastasis of cancer cells.[22,23] Paclitaxel is a milestone natural drug that has been found to have a special therapeutic effect and action mechanism for breast cancer and ovarian cancer.[24] It stabilizes microtubule polymers and prevents their division, and

Received: May 8, 2022
Accepted: July 27, 2022
Published: August 5, 2022

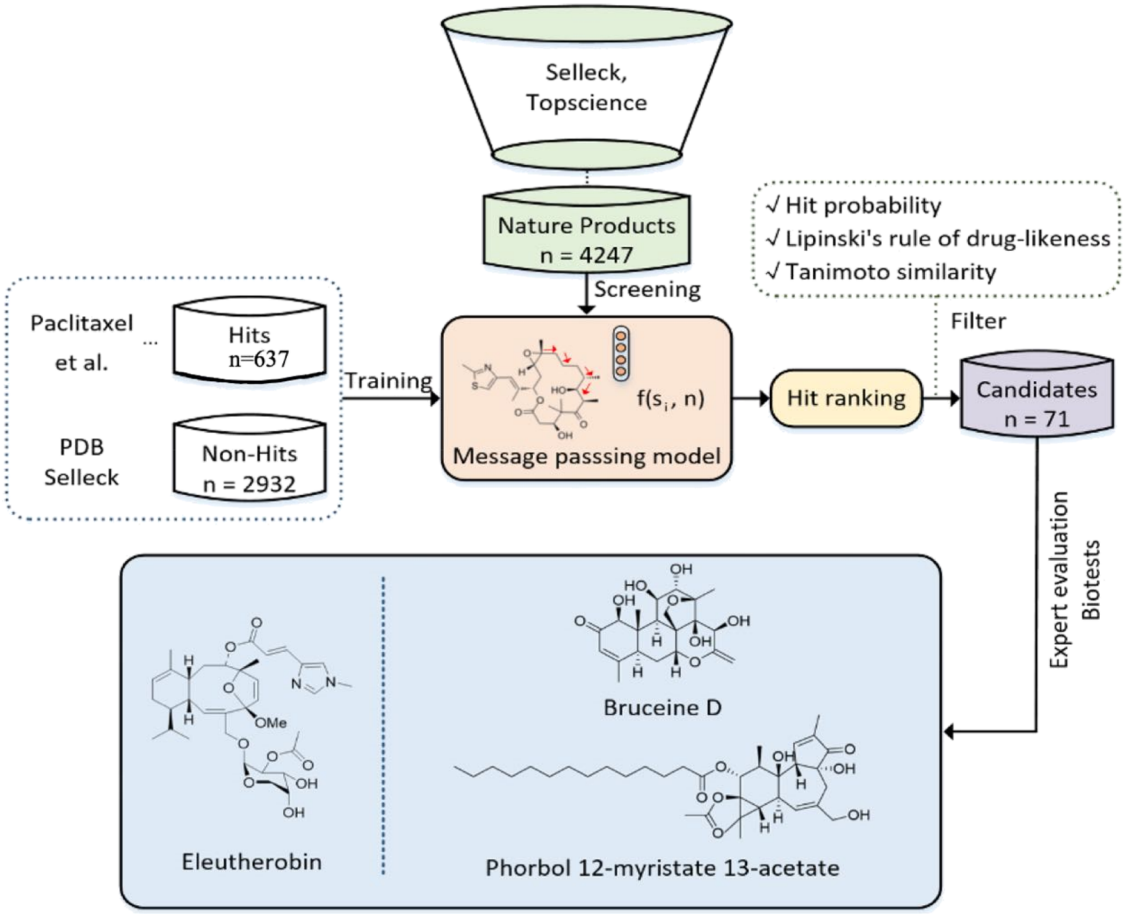

Figure 1. Flowchart of the AI-assisted discovery in natural products. A comprehensive hit dataset and a non-hit dataset were used to train a deep learning model. The trained model was used to screen a selected nature product dataset. The compounds were ranked by hit probability. The ranked compounds were further filtered to obtain the candidate dataset. Expert evaluated the candidates, conducted biotests, and identified three highly potent natural products of eleutherobin, bruceine D, and phorbol 12-myristate 13-acetate.

chromosomes cannot achieve medium-term spindle configuration. This blocks the progression of mitosis, prolongs the activation of mitosis, triggers apoptosis, or reverses the G_0 phase of the cell cycle without cell division. Paclitaxel has been one of the most successful anti-cancer drugs in the last 30 years.[25] Ixabepilone is a novel cytotoxic compound derivate produced by myxomycetes.[26] Similar to paclitaxel, it also inhibits tubulin depolymerization and shows strong anti-tumor activity in P-glycoprotein-expressing multidrug-resistant tumors. These star drugs from natural products have inspired natural product chemists to continue their research for potential molecules with better activity and fewer side effects. Considering the significant advances of deep learning in drug discovery, it is particularly interesting to utilize deep learning to develop a new generation of tubulin inhibitors from the vast natural product library. In this study, we aim to adopt deep learning approaches to screen natural product libraries for potent β-microtubule inhibitors. The overall flowchart of this study is illustrated in Figure 1.

We assembled a hit dataset of 637 known β-tubulin inhibitors and a non-hit dataset of 2932 molecules, including tyrosine kinase inhibitors, small molecular immuno-oncology compounds, and angiogenesis-related compounds. The hit and non-hit datasets were used to train a directed message passing neural network (DMPNN).[27,28] An additional group of 4247 compounds was retrieved from public natural product libraries to form the natural product dataset. The trained DMPNN combined with various molecular fingerprints were adopted to virtual screen the natural product dataset. The performance of DMPNN, and three enhanced DMPNN were evaluated and additional machine learning algorithms were compared. All candidates screened by DMPNN were ranked by hit probability and further filtered by hit probability, Lipinski's rule of drug-likeness, and Tanimoto similarity. Potential hits were manually checked, and three natural products were found as potent β-microtubule inhibitors. Among them, eleutherobin was identified as β-tubulin polymerization inhibitor reported in previous studies,[29,30] and for the first time, bruceine D (BD) and phorbol 12-myristate 13-acetate (PMA) were identified as active β-microtubule inhibitors by experimental validation. Current work highlights the significant potential of applying deep learning-based virtual screening approaches in drug discovery from natural products.

2. RESULTS AND DISCUSSION

2.1. Identification of Eleutherobin, BD, and PMA as β-Microtubule Inhibitors. We first used the compounds of the hit dataset and non-hit dataset to train the adopted DMPNN model. The performance of DMPNN models on an independent testing set were summarized in Table 1 and Figure 2. Additionally, we also systematically evaluated other machine learning algorithms (see Supporting Information,

https://doi.org/10.1021/acsomega.2c02854
ACS Omega 2022, 7, 28334−28341

Table 1. Performance of DMPNN Models (2D Normalized Features, Morgan Fingerprint with Bit Vector Features, Morgan Fingerprint Count Features, No Appended Features) in an Independent Testing Dataset

DMPNN models	AUC	ACC	precision	recall
2D normalized features	0.9962	0.9600	0.9832	0.9360
Morgan fingerprint with bit vector features	0.9867	0.9160	0.9906	0.8400
Morgan fingerprint count features	0.9859	0.9120	0.9813	0.8400
No appended features	0.9915	0.9280	0.9908	0.8640

Tables S5 and S6 and Figures S1 and S2). The trained model was used to screen the natural product dataset for potential hits of β-microtubule inhibitors. The screened compounds were later filtered according to hit probability, Lipinski's rule of drug-likeness, and molecular similarity. The qualified compounds were manually evaluated and surveyed in literatures. Those candidate compounds were further investigated for anti-tumor activity and β-tubulin polymerization inhibition activity. Finally, three natural products, including eleutherobin, BD, and PMA, were identified as β-microtubule inhibitors (Figure 3).

2.2. BD and PMA Inhibit Microtubule Assembly in MDA-MB-231 Cells. It has been shown that BD and PMA elicit anti-proliferative effects in multiple types of cancer.[31−34] Firstly, we found that BD and PMA exhibited potent anti-proliferative activity (IC_{50} values of 10.8 and 10.6 μM, respectively) in a dose-dependent manner in MDA-MB-231 cells by MTT assay (Figure 4a). Accordingly, 10 BD and 10 μM PMA were used in subsequent experiments. Next, we performed an immunofluorescence assay to confirm whether BD and PMA could inhibit microtubule assembly. We observed β-tubulin was abnormally accumulated, and the fluorescence intensity was significantly reduced in MDA-MB-231 cells after treatment with BD or PMA (Figure 4b,c). These results indicate that BD and PMA may be potential β-microtubule inhibitors.

2.3. BD and PMA Induce Cell Cycle Arrest in MDA-MB-231 Cells. Previous studies have shown that BD and PMA are potent inducers of cell cycle arrest.[31,35] Moreover, microtubules are essential in the mitosis process, and microtubule inhibitors could disturb the progress of the cell cycle.[36] Therefore, we verified whether BD and PMA could similarly induce cell cycle arrest in MDA-MB-231 cells. Accordingly, we found that BD induced S phase arrest and PMA induced G_0/G_1 phase arrest (Figure 5a,b). Furthermore, as the key cell cycle regulators, the expression of CDK1, CDK2, and cyclin E was inhibited (Figure 5c,d), which further confirmed the above results. These results suggest that BD and PMA induce cell cycle arrest, although their respective periods of action are different.

2.4. BD and PMA Induce Apoptosis in MDA-MB-231 Cells. To ascertain whether apoptosis was associated with the anti-tumor effects of BD and PMA, we evaluated their apoptotic ratio in MDA-MB-231 cells using annexin V/PI double staining. The results showed that a significant increase in early apoptotic cells in the presence of BD and PMA. Interestingly, PMA induced a higher rate of apoptosis compared with BD, indicating that PMA could elicit more obvious apoptosis (Figure 6a,b). Additionally, we detected the expression of apoptosis-related proteins such as Bax, Bcl-2, and caspase-3 in MDA-MB-231 cells, which suggested the activation of the apoptotic pathway (Figure 6c,d). Taken together, the above results demonstrate that BD and PMA elicit anti-proliferative effects via inducing apoptosis in MDA-MB-231 cells.

3. CONCLUSIONS

In conclusion, we systematically developed a deep learning framework to screen natural products for potential β-microtubule inhibitors. In the obtained hits, eleutherobin was found in agreement with previous reports.[29,30] Another two compounds, BD and PMA were confirmed by experimental

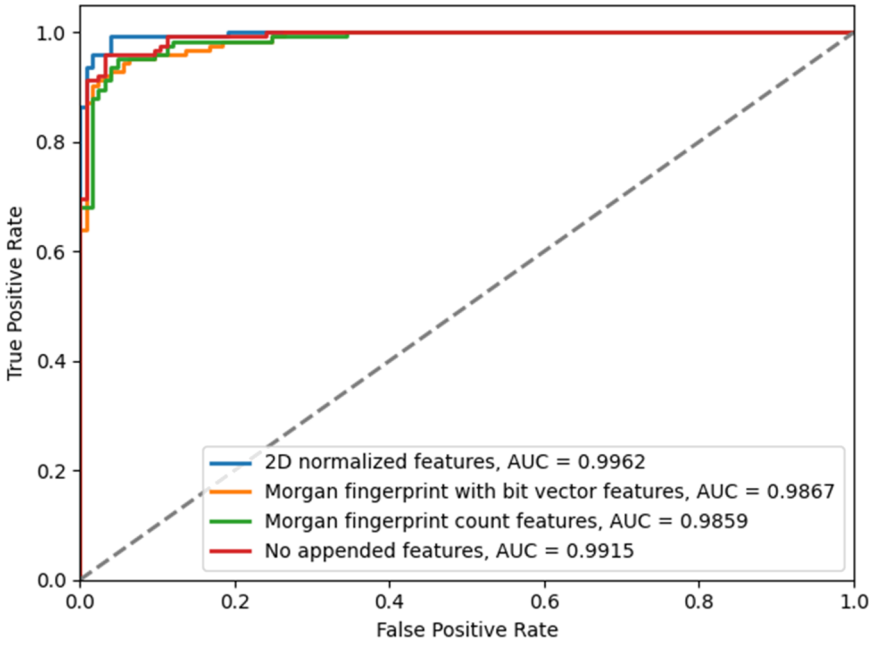

Figure 2. ROC diagrams of four DMPNN models (2D normalized features, Morgan fingerprint with bit vector features, Morgan fingerprint count features, no appended features) in an independent testing dataset.

https://doi.org/10.1021/acsomega.2c02854
ACS Omega 2022, 7, 28334−28341

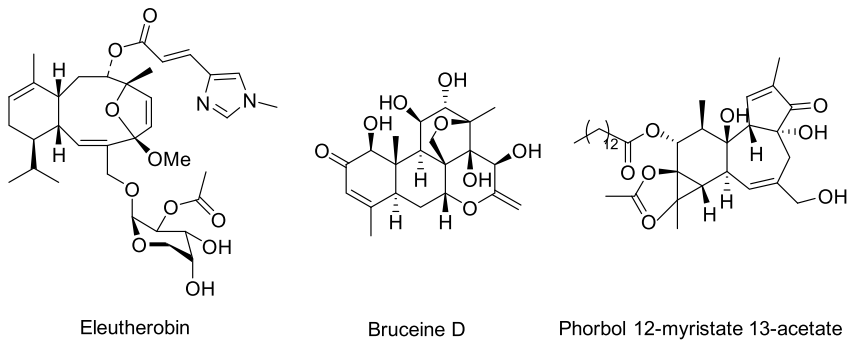

Figure 3. The structures of the three potential inhibitors are eleutherobin, bruceine D, and phorbol 12-myristate 13-acetate, which are screened by the DL model. Eleutherobin has been confirmed the capability of inducing β-tubulin polymerization, which is similar to paclitaxel.[29,30] The successful identification of eleutherobin demonstrated the effectiveness of our deep learning approach in screening for β-tubulin polymerization inhibitors.

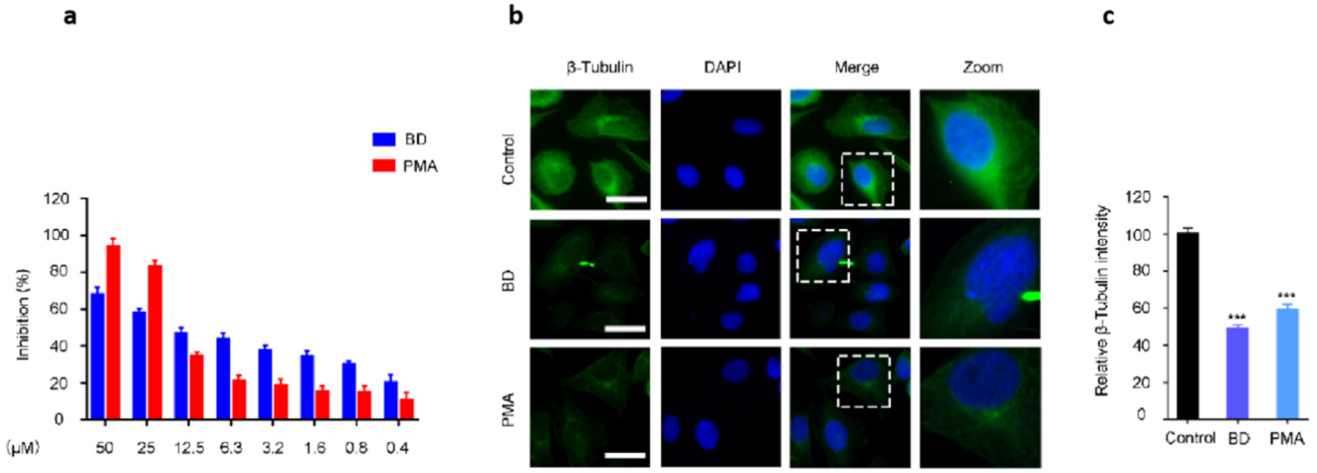

Figure 4. Results of MTT assay and images of immunofluorescence confocal microscopy for bruceine D, and phorbol 12-myristate 13-acetate. (a) MTT assays performed to measure the anti-proliferative potency of bruceine D and phorbol 12-myristate 13-acetate against MDA-MB-231 cell. (b, c) Immunofluorescence confocal microscopy images of MDA-MB-231 cells treated with 10 μM bruceine D and 10 μM phorbol 12-myristate 13-acetate for 24 h, respectively. The nuclei and microtubules have been labeled with DAPI and β-tubulin, respectively. Representative images with quantification of β-tubulin intensity were shown. Scale bar, 20 μm. ***$P < 0.001$. Statistical significance was compared with respective control groups.

validation, demonstrating potential β-microtubule inhibition activity.

In addition, there is still room in the present work for further improvement with future efforts. Firstly, the datasets could be further expanded to include more molecules in the hit and non-hit datasets to train the deep learning model, as well as more candidates in the natural product dataset. Ideally, more molecules of diversified chemical structures would enable the model to further explore the chemical space, hence increasing the chances of discovering new valid compounds. With the availability of libraries of massive compounds and natural products, the pipeline proposed in this work can be easily applied to these libraries for better model training and screening. Secondly, the model can be pre-trained using other massive molecules before being trained by the specifically assembled hit and non-hit datasets. This approach could mitigate the cold start issues in deep learning. Thirdly, this work adopted the DMPNN model, which is not a generative model. It's possible and easy to adopt generative models to replace the DMPNN model in our pipeline. Unlike the DMPNN, which is a non-generative model, generative models can be trained to learn the latent representation of molecules, which allows these models to screen molecules for desired properties. Moreover, using generative models could generate new molecular structures beyond the explored chemical space.

Overall, the results of this study demonstrate that our deep learning-based virtual screening pipeline could successfully identify three natural compounds as highly potent β-microtubule inhibitors. This work shows the encouraging potential of applying deep learning approaches in drug discovery, especially from abundant natural products.

4. EXPERIMENTAL SECTION

4.1. Hit Dataset Preparation. We systematically searched compounds databases for hits of β-microtubule inhibitors. In Selleck (a commercial database, selleckchem.com), we identified 22 microtubule-associated compounds. Furthermore, we surveyed published literature for FDA-approved drugs and compounds entering clinical trials and identified four compounds, including paclitaxel.[37−40] In addition to these 26 compounds entering clinical trials, we also considered compounds from pre-clinical trials which demonstrated as potential β-microtubule inhibitors. Specifically, in databases of ChEMBL, PDB, and ZINC15, we identified 611 active compounds with potential capability. In total, 637 compounds

https://doi.org/10.1021/acsomega.2c02854
ACS Omega 2022, 7, 28334−28341

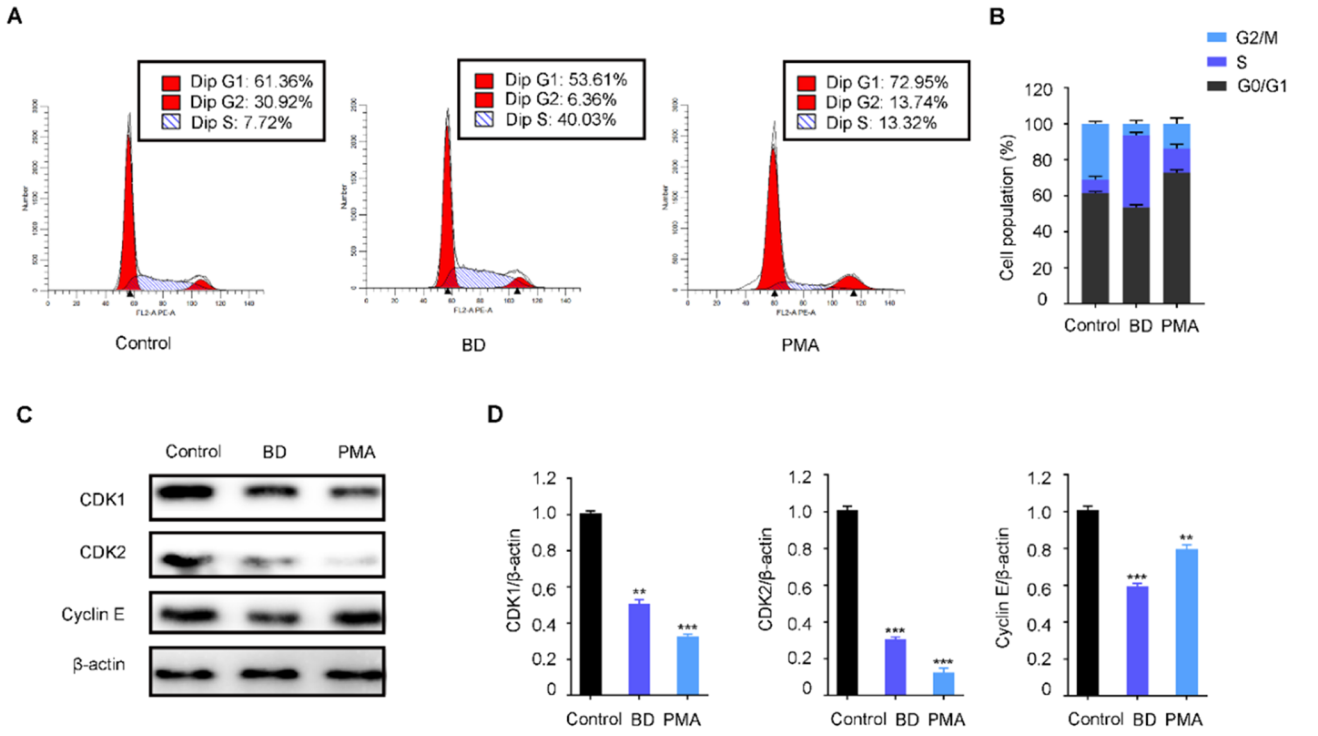

Figure 5. Cell cycle analysis after bruceine D and phorbol 12-myristate 13-acetate treatment and Western blot analysis after bruceine D and phorbol 12-myristate 13-acetate treatment. (a, b) MDA-MB-231 cell treated with 10 μM bruceine D and 10 μM phorbol 12-myristate 13-acetate for 24 h, respectively. Cell cycle analysis was performed with propidium iodide. (c, d) Western blot analysis of CDK1, CDK2, and cyclin E in MDA-MB-231 cell treated with 10 μM bruceine D and 10 μM phorbol 12-myristate 13-acetate for 24 h, respectively. Relative CDK1, CDK2, and cyclin E expression levels were quantified by normalization to β-actin. $^{**}P < 0.01$, $^{***}P < 0.001$. Statistical significance compared with respective control groups.

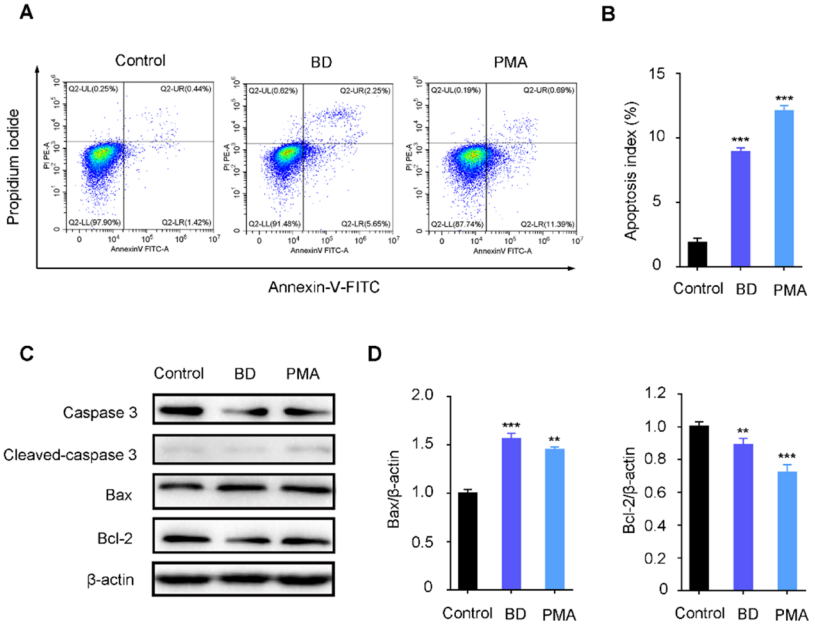

Figure 6. Apoptosis analysis of MDA-MB-231cells treated with bruceine D and phorbol 12-myristate 13-acetate and Western blot analysis. (a, b) MDA-MB-231 cells were treated with 10 μM bruceine D and 10 μM phorbol 12-myristate 13-acetate for 24 h, respectively. Apoptosis ratios were determined by flow cytometry analysis of annexin V/PI double staining. Representative images and quantification of apoptosis were shown. (c, d) Western blot analysis of caspase 3, cleaved caspase 3, Bax and Bcl-2 in MDA-MB-231 cell treated with 10 μM bruceine D and 10 μM phorbol 12-myristate 13-acetate for 24 h, respectively. Relative Bax and Bcl-2 expression levels were quantified by normalization to β-actin. $^{**}P < 0.01$, $^{***}P < 0.001$. Statistical significance was compared with respective control groups.

were included to assemble the hit dataset (see Supporting Information, Table S1).

4.2. Non-Hit Dataset Preparation. In order to establish the non-hit dataset, we searched ChEMBL, PDB, and Selleck

https://doi.org/10.1021/acsomega.2c02854
ACS Omega 2022, 7, 28334−28341

databases for FDA-approved drugs and activate compounds that were not reported as active β-microtubule inhibitors. As a result, we collected 2932 compounds to assemble the non-hit compounds (see Supporting Information, Table S2).

4.3. Natural Products Dataset Preparation. We manually searched compounds of natural products from Selleck and Topscience databases. In total, 4247 compounds were selected, including sesquiterpene, diterpenoid, and those alkaloids which our group investigated in previous studies. Therefore, these compounds represent diverse chemical structures and bioactivities. The selected compounds formed the natural product dataset for later screening (see Supporting Information, Table S3).

4.4. Model Implementation. To utilize the information of molecular structures, a message-passing neural network (MPNN) framework was used in this study, namely, the directed message passing neural network (DMPNN)[27] was adopted. In DMPNN, properties of atoms and bonds are encoded as feature vectors with which multiple rounds of message passing operations are conducted over the molecular graph. In each round of message passing, the feature vectors were updated by aggregating messages from neighbors. After certain rounds of convolutional embeddings, the global descriptor in the form of a feature vector was obtained for the given molecule, with which molecular properties could be analyzed and predicted using conventional machine learning approaches. Thanks to the impactful success in search potent antibiotics, DMPNN has attracted significant attention with emerging applications of chemical property prediction, drug discovery, and structure characterization analysis.[41−43]

Extended on the learned descriptor for the input molecule by the DMPNN, we appended additional molecular fingerprints obtained using RDKit (http://rdkit.org/), namely the binary Morgan fingerprints, count-based Morgan fingerprints, and RDKit 2D normalized fingerprints to further enhance the information on the DMPNN descriptor. Using the basic DMPNN descriptor and the three enhanced fingerprint combinations, we classify the input molecules against their hit/non-hit labels. Finally, the hit probability indicating the likeliness of inhibiting β-tubulin for a given molecule was obtained for later filtering. For simplicity, the basic hyperparameters were adopted from the original implementation of DMPNN.[27,28]

4.5. Model Training and Screening. The hit and non-hit datasets were used to form the training dataset to train the DMPNN architecture. As described above, for each input molecule, using the basic DMPNN descriptor and the three enhanced descriptors, the hit probability and cross-entropy of binary classification were calculated against the ground truth. The weights in the DMPNN were updated using back-propagations. Once all molecules from the hit and non-hit datasets were input into the models, the DMPNN was trained and hence learned the capability of discriminating hits from non-hits. Following the training, we input all the molecules in the natural product dataset into the trained DMPNN, and the hit probabilities were obtained using the basic DMPNN descriptor and the three enhanced descriptors. We ranked all candidates and focused on the top molecules with a predicted hit probability larger than 0.8. This screening significantly narrowed the candidate dataset.

4.6. Molecule Similarity. In order to obtain diversified chemical structures in selected compounds, we removed molecules that were structurally similar to the molecules in the hit dataset. We calculated the Tanimoto similarity coefficients using RDKit. The coefficient of two given molecules is obtained by calculating the distance between the molecular fingerprints of the two molecules. Candidate compounds having a Tanimoto similarity coefficient larger than the cut-off of 0.4 to any of the molecules in the hit dataset were filtered.

4.7. Lipinski's Rule of Drug-Likeness. The top molecules with optimal hit probability obtained in the initial screening using DMPNN were further analyzed using Lipinski's rule of drug-likeness. In this study, we set filters as $250 \leq$ molecular weight ≤ 500, log$P \leq 5$, the amount of hydrogen bond donors ≤ 5, the amount of hydrogen bond acceptors ≤ 10. By applying the rules, we further focused on an even smaller group of candidates, allowing manual evaluations.

4.8. Cell Culture, Antibodies, and Reagents. Cells were purchased from American Type Culture Collection (ATCC, Manassas, VA, USA) and were cultured in DMEM with 10% fetal bovine serum and incubated with 5% CO2. Antibodies used in this study were as follows: caspase 3 (9662, CST), Bax (5023, CST), Bcl-2 (2870, CST), CDK1 (201008, Abcam), CDK2 (2546, CST), cyclin E (4129, CST), β-actin (3700, CST), β-tubulin (2128, CST). Compound BD and PMA were purchased from MedChemExpress.

4.9. Cell Viability Assay. Cell viability was measured by the MTT assay. MDA-MB-231 cell was dispensed in 96-well plates at a density of 7×10^3 cells/ml for 24 h. Then, cells were treated with different concentrations of compounds for 24 h.

4.10. Apoptosis and Cell Cycle Assays. For apoptosis assay, MDA-MB-231 cell was treated with 10 μM BD and 10 μM PMA for 24 h, respectively. Apoptosis ratios were determined by flow cytometry analysis of annexin V/PI double staining. For cell cycle detection, MDA-MB-231 cell was treated with 10 μM BD and 10 μM PMA for 24 h, respectively. Then, the cell cycle distribution was determined by flow cytometry analysis of PI staining.

4.11. Immunofluorescence Analysis. The MDA-MB-231 cell was incubated with β-tubulin (1200) in PBS containing 1% BSA incubated overnight at 4 °C, followed by the addition of fluorescent-labeled secondary antibodies (Alexa Fluor 488, ab150077) for 1 h at room temperature. Images were captured using a confocal laser canning microscopy (Zeiss).

4.12. Immunoblotting Analysis. Adherent and floating cells were collected and lysed by lysis buffer at 4 °C for 30 min. The protein content of the supernatant was quantified by Bio-Rad DC protein assay (Bio-Rad Laboratories, Hercules, CA, USA). Equal amounts of the total protein were separated by 15% SDS-PAGE and transferred to PVDF membranes, followed by primary antibodies and HRP-conjugated secondary antibodies. Quantification of immunoblot was performed by ImageJ 1.8.0.

4.13. Data Availability. Data are available within the article and supplementary files. All other data that support the findings of the study are available from the corresponding author upon reasonable request.

4.14. Code Availability. The source codes of DMPNN architecture are provided in the paper.[27] Python codes for the pipeline are available on GitHub (https://github.com/gracewang723/chemprop).

https://doi.org/10.1021/acsomega.2c02854
ACS Omega 2022, 7, 28334−28341

■ ASSOCIATED CONTENT

Supporting Information

The Supporting Information is available free of charge at https://pubs.acs.org/doi/10.1021/acsomega.2c02854.

Molecules of hit dataset, molecules of non-hit dataset, natural product dataset, candidate dataset, list of additional machine learning algorithms, performance of additional machine learning algorithms in an independent testing dataset, ROC diagrams of additional machine learning algorithms using the RDKit topological fingerprint, and ROC diagrams of additional machine learning algorithms using the RDKit Morgan fingerprint (PDF)

■ AUTHOR INFORMATION

Corresponding Authors

Hai-Ning Song − *Department of Pharmacy, The Third People's Hospital of Chengdu and College of Medicine, Southwest Jiaotong University, Chengdu 610031, PR China*; Email: songhaining@126.com

Yong Tang − *School of Computer Science and Engineering, University of Electronic Science and Technology of China, Chengdu 610054, PR China*; Email: tangyong@uestc.edu.cn

Feng Gao − *School of Life Science and Engineering, Southwest Jiaotong University, Chengdu 610031, PR China*; orcid.org/0000-0001-9436-681X; Email: gaof@swjtu.edu.cn

Authors

Xiao-Nan Jia − *School of Life Science and Engineering, Southwest Jiaotong University, Chengdu 610031, PR China*

Wei-Jia Wang − *School of Computer Science and Engineering, University of Electronic Science and Technology of China, Chengdu 610054, PR China*

Bo Yin − *School of Life Science and Engineering, Southwest Jiaotong University, Chengdu 610031, PR China*

Lin-Jing Zhou − *School of Information and Software Engineering, University of Electronic Science and Technology of China, Chengdu 610054, PR China*

Yong-Qi Zhen − *School of Life Science and Engineering, Southwest Jiaotong University, Chengdu 610031, PR China*

Lan Zhang − *School of Life Science and Engineering, Southwest Jiaotong University, Chengdu 610031, PR China*

Xian-Li Zhou − *School of Life Science and Engineering, Southwest Jiaotong University, Chengdu 610031, PR China*; orcid.org/0000-0002-1690-0578

Complete contact information is available at: https://pubs.acs.org/10.1021/acsomega.2c02854

Author Contributions

⊥X.-N.J., W.-J.W., and B.Y. contributed equally to this work.

Notes

The authors declare no competing financial interest.

■ ACKNOWLEDGMENTS

This study is supported by the Key R&D Program of the Ministry of Science and Technology of the People's Republic of China (2020YFF0305104), National Natural Science Foundation of China (31570341 and 31870329), Key Research and Development Project of the Science & Technology Department of Sichuan Province (2020YFS0324), and Fundamental Research Funds for the Central Universities of China (YGJH2020-LY06).

■ REFERENCES

(1) Newman, D. J.; Cragg, G. M. Natural Products as Sources of New Drugs from 1981 to 2014. *J. Nat. Prod.* **2016**, *79*, 629−661.

(2) Newman, D. J.; Cragg, G. M. Natural Products as Sources of New Drugs over the 30 Years from 1981 to 2010. *J. Nat. Prod.* **2012**, *75*, 311−335.

(3) Jeon, J.; Kang, S.; Kim, H. U. Predicting Biochemical and Physiological Effects of Natural Products from Molecular Structures Using Machine Learning. *Nat. Prod. Rep.* **2021**, *38*, 1954−1966.

(4) Ballester, P. Machine Learning for Molecular Modelling in Drug Design. *Biomolecules* **2019**, *9*, 216.

(5) Lo, Y.-C.; Rensi, S. E.; Torng, W.; Altman, R. B. Machine Learning in Chemoinformatics and Drug Discovery. *Drug Discovery Today* **2018**, *23*, 1538−1546.

(6) Zhang, L.; Tan, J.; Han, D.; Zhu, H. From Machine Learning to Deep Learning: Progress in Machine Intelligence for Rational Drug Discovery. *Drug Discovery Today* **2017**, *22*, 1680−1685.

(7) Chen, H.; Engkvist, O.; Wang, Y.; Olivecrona, M.; Blaschke, T. The Rise of Deep Learning in Drug Discovery. *Drug Discovery Today* **2018**, *23*, 1241−1250.

(8) Mak, K.-K.; Pichika, M. R. Artificial Intelligence in Drug Development: Present Status and Future Prospects. *Drug Discovery Today* **2019**, *24*, 773−780.

(9) Vamathevan, J.; Clark, D.; Czodrowski, P.; Dunham, I.; Ferran, E.; Lee, G.; Li, B.; Madabhushi, A.; Shah, P.; Spitzer, M.; Zhao, S. Applications of Machine Learning in Drug Discovery and Development. *Nat. Rev. Drug Discov.* **2019**, *18*, 463−477.

(10) Rifaioglu, A. S.; Atalay, R. C.; Kahraman, D. C.; Dogan, T.; Martin, M.; Atalay, V. MDeePred: Novel Multi-Channel Protein Featurization for Deep Learning-Based Binding Affinity Prediction in Drug Discovery. *Bioinformatics* **2021**, *37*, 693−704.

(11) Galushka, M.; Swain, C.; Browne, F.; Mulvenna, M. D.; Bond, R.; Gray, D. Prediction of Chemical Compounds Properties Using a Deep Learning Model. *Neural. Comput. Appl.* **2021**, *33*, 13345−13366.

(12) Ma, B. A.; Terayama, K.; Matsumoto, S.; Isaka, Y.; Sasakura, Y.; Iwata, H.; Araki, M.; Okuno, Y. Structure-Based de Novo Molecular Generator Combined with Artificial Intelligence and Docking Simulations. *J. Chem. Inf. Model.* **2021**, *61*, 3304−3313.

(13) Madaj, R.; Geoffrey, B.; Sanker, A.; Valluri, P. P. Target2DeNovoDrug: A Novel Programmatic Tool for in Silico-Deep Learning Based de Novo Drug Design for Any Target of Interest. *J. Biomol. Struct. Dyn.* **2021**, 1.

(14) Krishnan, S. R.; Bung, N.; Bulusu, G.; Roy, A. Accelerating De Novo Drug Design against Novel Proteins Using Deep Learning. *J. Che. Inf. Model.* **2021**, *61*, 621−630.

(15) Abdullah, M.; Guruprasad, L. Identification of 3D Motifs Based on Sequences and Structures for Binding to CFI-400945, and Deep Screening-Based Design of New Lead Molecules for PLK-4. *Chem. Biol. Drug Des.* **2021**, *98*, 522−538.

(16) Crunkhorn, S. Deep Learning Framework for Repurposing Drugs. *Nat. Rev. Drug Discovery* **2021**, *20*, 100−100.

(17) Issa, N. T.; Stathias, V.; Schurer, S.; Dakshanamurthy, S. Machine and Deep Learning Approaches for Cancer Drug Repurposing. *Semin. Cancer Biol.* **2021**, *68*, 132−142.

(18) Liu, R.; Wei, L.; Zhang, P. A Deep Learning Framework for Drug Repurposing via Emulating Clinical Trials on Real-World Patient Data. *Nat. Mach. Intell.* **2021**, *3*, 68−75.

(19) Fang, C.; Shen, Z.; Zhang, Z.; You, X.; Zhang, C. Synthesizing a Neuron Using Chemical Reactions. In *2018 IEEE International Workshop on Signal Processing Systems (SiPS)*; IEEE: New York, 2018; pp. 187−192.

(20) Liu, Z.; Huang, D.; Zheng, S.; Song, Y.; Liu, B.; Sun, J.; Niu, Z.; Gu, Q.; Xu, J.; Xie, L. Deep Learning Enables Discovery of Highly Potent Anti-Osteoporosis Natural Products. *Eur. J. Med. Chem.* **2021**, *210*, 112982.

(21) Delijewski, M.; Haneczok, J. AI Drug Discovery Screening for COVID-19 Reveals Zafirlukast as a Repurposing Candidate. *Med. Drug Discovery* **2021**, *9*, 100077.
(22) Xu, L.; Wang, W.; Meng, T.; Ma, L.-P.; Tong, L.-J.; Shen, J.-K.; Wang, Y.-Q.; Miao, Z.-H. New Microtubulin Inhibitor MT189 Suppresses Angiogenesis via the JNK-VEGF/VEGFR2 Signaling Axis. *Cancer Lett.* **2018**, *416*, 57−65.
(23) Islam, M. N.; Iskander, M. N. Microtubulin Binding Sites as Target for Developing Anticancer Agents. *Mini-Rev. Med. Chem.* **2004**, *4*, 1077−1104.
(24) Brito, D. A.; Yang, Z.; Rieder, C. L. Microtubules Do Not Promote Mitotic Slippage When the Spindle Assembly Checkpoint Cannot Be Satisfied. *Int. J. Biochem. Cell Biol.* **2008**, *182*, 623−629.
(25) Adams, D. J.; Wahl, M. L.; Flowers, J. L.; Sen, B.; Colvin, M.; Dewhirst, M. W.; Manikumar, G.; Wani, M. C. Camptothecin Analogs with Enhanced Activity against Human Breast Cancer Cells. II. Impact of the Tumor PH Gradient. *Cancer Chemother. Pharmacol.* **2006**, *57*, 145.
(26) Waight, A. B.; Bargsten, K.; Doronina, S.; Steinmetz, M. O.; Prota, A. E. Structural Basis of Microtubule Destabilization by Potent Auristatin Anti-Mitotics. *PLoS One* **2016**, *11*, No. e0160890.
(27) Yang, K.; Swanson, K.; Jin, W.; Coley, C.; Eiden, P.; Gao, H.; Guzman-Perez, A.; Hopper, T.; Kelley, B.; Mathea, M.; Palmer, A.; Settels, V.; Jaakkola, T.; Jensen, K.; Barzilay, R. Analyzing Learned Molecular Representations for Property Prediction. *J. Chem. Inf. Model.* **2019**, *59*, 3370−3388.
(28) Stokes, J. M.; Yang, K.; Swanson, K.; Jin, W.; Cubillos-Ruiz, A.; Donghia, N. M.; MacNair, C. R.; French, S.; Carfrae, L. A.; Bloom-Ackermann, Z.; Tran, V. M.; Chiappino-Pepe, A.; Badran, A. H.; Andrews, I. W.; Chory, E. J.; Church, G. M.; Brown, E. D.; Jaakkola, T. S.; Barzilay, R.; Collins, J. J. A Deep Learning Approach to Antibiotic Discovery. *Cell* **2020**, *180*, 688−702.e13.
(29) Sosonyuk, S. E.; Peshich, A.; Tutushkina, A. V.; Khlevin, D. A.; Lozinskaya, N. A.; Gracheva, Y. A.; Glazunova, V. A.; Osolodkin, D. I.; Semenova, M. N.; Semenov, V. V.; Palyulin, V. A.; Proskurnina, M. V.; Shtil, A. A.; Zefirov, N. S. Synthesis and Cytotoxicity of Novel Simplified Eleutherobin Analogues as Potential Antitumour Agents. *Org. Biomol. Chem.* **2019**, *17*, 2792−2797.
(30) Long, B. H.; Carboni, J. M.; Wasserman, A. J.; Cornell, L. A.; Casazza, A. M.; Jensen, P. R.; Lindel, T.; Fenical, W.; Fairchild, C. R. Eleutherobin, a Novel Cytotoxic Agent That Induces Tubulin Polymerization, Is Similar to Paclitaxel (Taxol (R)). *Cancer Res.* **1998**, *58*, 1111−1115.
(31) Li, L.; Dong, Z.; Shi, P.; Tan, L.; Xu, J.; Huang, P.; Wang, Z.; Cui, H.; Yang, L. Bruceine D Inhibits Cell Proliferation Through Downregulating LINC01667/MicroRNA-138-5p/Cyclin E1 Axis in Gastric Cancer. *Front. Pharmacol.* **2020**, *11*, 584920.
(32) Wang, S.; Hu, H.; Zhong, B.; Shi, D.; Qing, X.; Cheng, C.; Deng, X.; Zhang, Z.; Shao, Z. Bruceine D Inhibits Tumor Growth and Stem Cell-like Traits of Osteosarcoma through Inhibition of STAT3 Signaling Pathway. *Cancer Med.* **2019**, *8*, 7345−7358.
(33) Kim, J.; Lee, D. H.; Badamtsetseg, B.; Lee, S.; Kim, S. A. Anti-Proliferative Effect of Allium Senescens L. Extract in Human T-Cell Acute Lymphocytic Leukemia Cells. *Molecules* **2021**, *26*, 942.
(34) Zhang, Y.; Liu, D.; Xue, F.; Yu, H.; Wu, H.; Cui, X.; Zhang, X.; Wang, H. Anti-Malignant Ascites Effect of Total Diterpenoids from Euphorbiae Ebracteolatae Radix Is Attributable to Alterations of Aquaporins via Inhibiting PKC Activity in the Kidney. *Molecules* **2021**, *26*, 942.
(35) Tian, F.; Tong, M.; Li, Z.; Huang, W.; Jin, Y.; Cao, Q.; Zhou, X.; Tong, G. The Effects of Orientin on Proliferation and Apoptosis of T24 Human Bladder Carcinoma Cells Occurs Through the Inhibition of Nuclear Factor-KappaB and the Hedgehog Signaling Pathway. *Med. Sci. Monit.* **2019**, *25*, 9547−9554.
(36) Steinmetz, M. O.; Prota, A. E. Microtubule-Targeting Agents: Strategies To Hijack the Cytoskeleton. *Trends Cell Biol.* **2018**, *28*, 776−792.
(37) Taraboletti, G.; Micheletti, G.; Rieppi, M.; Poli, M.; Turatto, M.; Rossi, C.; Borsotti, P.; Roccabianca, P.; Scanziani, E.; Nicoletti, M. I.; Bombardelli, E.; Morazzoni, P.; Riva, A.; Giavazzi, R. Antiangiogenic and Antitumor Activity of IDN 5390, a New Taxane Derivative. *Clin. Cancer Res.* **2002**, *8*, 1182−1188.
(38) Ono, C.; Takao, A.; Atsumi, R. Absorption, Distribution, and Excretion of DJ-927, a Novel Orally Effective Taxane, in Mice, Dogs, and Monkeys. *Biol. Pharm. Bull.* **2004**, *27*, 345−351.
(39) Dieras, V.; Limentani, S.; Romieu, G.; Tubiana-Hulin, M.; Lortholary, A.; Kaufman, P.; Girre, V.; Besenval, M.; Valero, V. Phase II Multicenter Study of Larotaxel (XRP9881), a Novel Taxoid, in Patients with Metastatic Breast Cancer Who Previously Received Taxane-Based Therapy. *Ann. Oncol.* **2008**, *19*, 1255−1260.
(40) Paller, C. J.; Antonarakis, E. S. Cabazitaxel: A Novel Second-Line Treatment for Metastatic Castration-Resistant Prostate Cancer. *Drug Des., Dev. Ther.* **2011**, *5*, 117−124.
(41) Withnall, M.; Lindelöf, E.; Engkvist, O.; Chen, H. Building Attention and Edge Message Passing Neural Networks for Bioactivity and Physical-Chemical Property Prediction. *Aust. J. Chem.* **2020**, *12*, 1.
(42) Karlov, D. S.; Popov, P.; Sosnin, S.; Fedorov, M. V. Message Passing Neural Networks Scoring Functions for Structure-Based Drug Discovery. *Artificial Neural Networks and Machine Learning - Icann 2019: Workshop and Special Sessions* **2019**, *11731*, 845−847.
(43) Jo, J.; Kwak, B.; Choi, H.-S.; Yoon, S. The Message Passing Neural Networks for Chemical Property Prediction on SMILES. *Methods* **2020**, *179*, 65−72.

https://doi.org/10.1021/acsomega.2c02854
ACS Omega 2022, 7, 28334−28341